Rodríguez-Hernández, MA.; Ramos, A.; San Emeterio Prieto, JL. (2011). Wavelet-based 2D fusing of ultrasonic pulse-echo traces measured from two arrays radiating orthogonal beams. Measurement Science and Technology. 22(10). doi:10.1088/0957-0233/22/10/105701.

Wavelet based 2D fusing of ultrasonic pulse-echo traces measured from two arrays radiating orthogonal beams

Miguel A. Rodríguez [1], Antonio Ramos [2], and J. L. San Emeterio [2]

[1] ITACA, Universitat Politècnica de València. Camino Vera s/n, 46022 Valencia. Spain
[2] Lab. "Ultrasonic Signals, Systems & Technologies" (CSIC). Serrano 144, 28006 Madrid. Spain

marodrig@upvnet.upv.es, aramos@ia.cetef.csic.es, jluis@ia.cetef.csic.es

Abstract

Ultrasonic measurements using orthogonal collimated beams provide both complementary and redundant information about internal parts of pieces or structures being tested, which must be fused. In this paper, a new wavelet-based digital processing technique which fuses ultrasonic pulse-echo traces obtained from several transducers located in two perpendicularly-coupled arrays is proposed. This is applied to accurately visualize the location of a small internal reflector by means of two dimensional (2D) displays.

A-scans are processed in wavelet domain and fused in a common 2D pattern. A mathematical expression of the resulting 2D signal-to-noise ratio (SNR) is derived, and its accuracy is confirmed using benchmark tests performed with simulated registers and real measurements acquired using a multi-channel laboratory prototype. The measurement system consists of two properly-coupled perpendicular arrays comprising 4 square pulsed transducers and electronic driving circuitry.

This technique improves 2D-SNR by a factor of twice the number of bands. In addition, good reflector location is obtained, since sub-millimeter 2D resolutions are achieved, despite only requiring eight ultrasonic channels. This good performance is confirmed by comparing the new wavelet fusing method with the two previously described techniques.

Keywords: Ultrasonics, Wavelets, Orthogonal ultrasonic beams, Echo-trace fusing, Digital signal processing, Non-destructive inspection.

PACS: 43.35Yb, 43.60.Hj

Submitted to: Measurement Science and Technology

1. Introduction. Background and Objectives

In quality control and material characterization applications, using conventional ultrasonic techniques for non invasive measurement in non destructive inspections (NDI), it is very difficult to detect certain types of internal reflectors or flaws. Classical instrumentation techniques, which use actuators orientated in only one plane, have limitations for some locations or orientations of the flaws.

There are applications where improvements in two-dimension flaw-location are achievable using several ultrasonic transducers. In fact, it is well-known that the use of more than one detection transducer provides complementary information about some types of reflector (Reguieg et al 2006, Engl and Meier 2002, Roy et al 1999, Chang and Hsieh 2002, Rodríguez et al 2004). These transducers can be located on the same plane (the so-called traditional linear or matrix phase-array cases) or on different planes, depending on the sample shape and the detection requirements. In such arrangements, different ultrasonic beams must be used to inspect the medium in a controlled way (Ramos and San Emeterio 2008) so as to obtain a set of coherent A-Scan ultrasonic traces. For scanning or focusing purposes (Ramos et al 1987, Ramos et al 1993, Ullate et al 1994), these A-scan traces are usually processed to increase the accuracy of the detection results over those obtained with single transducer echo-acquisition.

In any case, it is important to reduce the number of ultrasonic channels in order to minimize technological costs. Nevertheless, in conventional ultrasonic scanners for NDI, it is customary to overcome restrictions and increase resolution levels, in flaw detection, by increasing the number of ultrasonic channels, typically rising to several hundred of channels.

It should be noted that the detection capability depends not only on using sophisticated multi-channel electronic equipment and new signal processing tools. It may also depend on other important factors related to the geometry and propagation of the ultrasonic beams. Some physical limitations of the ultrasonic beams still exist for certain scanning angles (Chang and Hsieh 2002) and for complex particular geometries in industrial components, due to diffraction phenomena (Roy et al 1999). Efficient solutions to these types of problems remain to be solved, but there are several works oriented in this direction. Some attempts employ two transducers and additional digital processing of the echoes (Chang and Hsieh 2002), while others (with a bigger cost) are based on several arrays mounted over the piece under inspection (Engl and Meier 2002).

With the aim of lowering technological costs, some classical beam collimation solutions based on a reduced number of transducers (typically less than ten elemental apertures) and arranged in annular geometries have been proposed (Lu et al 1992, Castellanos et al 2010). These are based on ultrasonic emission from only one plane and require mechanical scanning in order to achieve a 2D display.

Various applications of overlapping beams generated from transducers mounted on different planes have been reported. Some of these use far-field transducers arranged in arrays so as to produce crossed beams (Defontaine et al 2004, Hillger et al 2004), while others use a system with few transducers and low-cost electronics in order to emit perpendicular beams (Meyer and Candy 2002).

Further research is required in order to find simple, low-cost and complete solutions to the abovementioned special 2D inspection problems. In particular, techniques for reducing the processing cost related to multiple ultrasonic radiations from perpendicular planes, using arrays consisting of a few radiators and working under near field conditions, are currently being investigated in the present authors' laboratories. At the same time, we are also developing digital signal processing tools for improving the SNR of the echoes acquired during the ultrasonic characterization of media with complex structure (Lázaro et al 2002, Rodríguez et al 2004a).

An alternative low-cost general scheme proposed for ultrasonic detection in Rodríguez 2003, will be improved and implemented in this paper to achieve a solution for accurate scanning and measurement of the location of possible reflectors inside an opaque piece. This solution only uses eight acoustic apertures located in perpendicular planes, and works with ultrasonic beams collimated in the near-field zone of each aperture, in contrast with the classical far-field imaging approaches. In this context, an efficient wavelet-based beam fusing option is tackled in this paper.

Novel ultrasonic orthogonal scanning techniques based on multiple near-field transducers have been developed in our laboratory. These techniques use different processing tools that combine the echo-traces acquired by several transducers located on two orthogonal planes. A-scan echo-information received from transducers in different planes, but corresponding to the same inspection area, is processed together before being displayed in a final integrated 2D pattern. This particular orthogonal scanning technique has been scarcely reported in the literature, although as a forerunner to this type of scanning, the inspection of a high-power laser with critical optical components, using ultrasonic transducers situated in perpendicular planes, is mentioned in Meyer and Candy 2002. In this case of testing an optical material, the backscattering noise can be interpreted as negligible, and a time-domain trace combination could be directly formed only using the arrival time of the ultrasonic echoes.

In other work proposed along the same inspection line, a test sample containing a single flaw was evaluated by transducers located on two perpendicular planes (Rodríguez et al 2004). Here, the trace combination was also performed in the time domain, but the receiving ultrasonic traces contained backscattering noise. Two fusion options were studied to noise reduction: one based on a 2D sum operator and the other using a 2D product operator. The SNR was used as a quality index to evaluate both methods, and the results showed better performance using the product operator; this effectively doubles the SNR value (expressed in dB). For this reason, in the following sections of this paper, we have always selected the product operator for the 2D fusing of our ultrasonic echo-traces.

In addition, a further complementary technique has been proposed (Rodríguez 2003). It combines the ultrasonic traces in the time-frequency domain, but using the Wigner-Ville transform. It takes into account both temporal and frequency information of the A-Scan traces and provides a better SNR than a direct combination in time domain (Rodríguez et al 2004). Nevertheless, this Wigner-Ville transform option has two disadvantages: a loss of linearity during the signal processing and a high computational processing time. Both aspects limit its application to simple flaws detection.

The main objective of this paper is to describe, implement and evaluate a new fusing technique for ultrasonic A-scans acquired from perpendicular planes. In this technique, the processing procedure is based on wavelet transform and 2D traces product, which allow fusing of ultrasonic near-field A-Scans in the time-scale plane with high quality results and a low associated computational cost. This procedure, which develops and implements an idea suggested and preliminary considered in (Rodríguez et al 2004b), is described and analyzed in detail along the following sections. Finally, the new technique is applied in order to achieve an accurate detection of an internal reflector by using a multi-step digital processing of synthetic and also experimental ultrasonic echo-traces. Some experiments also show very significant improvements in the resulting SNR after fusing.

In order to evaluate the performance of the proposed wavelet fusing technique, a multi-element ultrasonic prototype was disposed to generate eight orthogonal beams from two perpendicular aperture planes. Then, the echoes from the near-field zone of the transducers were measured. The performance of this fusing procedure was compared, in terms of the 2D-SNR improvement, with the two previously mentioned combination techniques proposed for these same inspection conditions: a) fusing in the time-domain using a Hilbert Transform (Rodríguez et al 2004), and b) fusing in the time-frequency domain using a Wigner-Ville Transform (Rodríguez 2003).

It should be noted that all these fusing techniques, discussed here, are distinct to the Split Spectrum Processing (SSP) technique (Newhouse et al 1982), which is used for noise reduction but without applying any trace fusing. It must also be noted that this near-field fusing procedure is different to classical array synthetic aperture techniques. In fact, these last techniques are based, as is well known, on the far-field approach for each elemental transducers employed in multi-channel echo-acquisition, and in addition they use other types of processing algorithms (SAFT**,** Synthetic Aperture Focusing Techniques) to emulate the classical focusing function.

Finally, 2D fused displays are generated in this paper, to show the results of processing synthetic and experimental ultrasonic echo-traces with the proposed wavelet based technique. In this way, the good spatial resolution capabilities of this technique are clearly demonstrated. So, for the first time in this type of bi-planar scanning, an extended dynamic range of 60 dB is used and reported for orthogonal beam inspection, in order to achieve an accurate 2D analysis of spatial resolutions; and uni-dimensional profiles are also analyzed at the maximum amplitude zone. Both display types allow secondary lobes to be detected and properly quantified in detail.

2. Experimental setup details

The laboratory test-piece used here to evaluate the proposed wavelet fusing technique consists of a small reflector placed inside a rectangular parallelepiped plastic block. The echographic inspection is performed using eight near-field beams radiated from two perpendicular external surfaces, with four transducers used per each surface for ultrasonic insonification and detection.

The general scheme of this experimental configuration is depicted in Figure 1, with horizontal (H1,

H2, H3, H4) and vertical (V1, V2, V3, V4) transducers denoted. A flaw is located in the intersection area of the horizontal beam from H3 and the vertical beam emitted by V2. When transducers H3 and V2 are driven, they receive echoes from the reflector mixed with spurious noise; whereas when the other transducers (H1, H2, H4, V1, V3 and V4) are driven they only receive noise. The resulting A-scans are fused to obtain a 2D representation of the reflector location. The details of the fussing process are described in section 4.

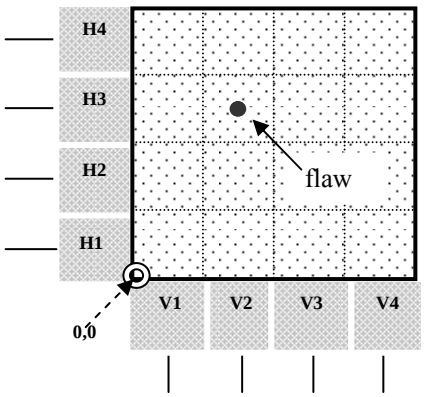

Figure 1. The geometry of the inspection configuration: detection of a single-flaw in a 2D arrangement using 8 transducers.

An experimental system with eight ultrasonic transceivers was designed in order to validate in laboratory (but, under real NDI conditions) the new flaw localization technique proposed for 2D trace fusing. It includes two 4 MHz piezoelectric linear arrays, each one with 4-elements emitter-receiver probes, which are controlled by a NDI equipment (Krautkramer USPC-2100) configured to work in the pulse-echo mode with receiving stages having dynamic ranges of 110 dB and a maximum effective digitalizing sampling rate of 200 MHz. A broadband gain of 44 dB for the echo-signals was used, and a sampling rate of 128 MHz was selected for signal acquisition of all the measured pulsed echoes considered for evaluation in this work. Other general characteristics of this NDI equipment are: pulse repetition rate of up to 10 KHz per channel, and 15 MHz of effective bandwidth in emission-reception.

The high-voltage pulser sections of this NDI equipment were set at around 400 Volts (which is the highest electric stimulation available in their driving units) measured when the output pulses are generated across a nominal resistive load of 100 Ohm. A relatively low value of 75 Ohm was selected for the E/R parallel damping resistances to provide a reasonable trade-off between a favorable initial SNR and a good bandwidth of the received echoes. Finally, the maximum value was selected for the driving spike energy level, depending on the selected discharging capacitor (Ramos et al 2008).

The two emitting-receiving ultrasonic arrays were coupled in right-angle configuration for our application; both arrays are composed of four broadband elemental transducer devices with working frequency bands centered around 4 MHz. To broaden the effective frequency bands were used individual matching layers in frontal sections adapted for acoustic coupling with plastic materials, and moderate mechanical backing sections in the other piezo-ceramic faces.

The elemental array radiators are 6 x 6 mm square apertures and were fabricated from our design specifications for particular orthogonal detection requirements in the selected test piece. Transducers would radiate from two external surfaces of the inspected pieces in the near field conditions along all the scanning depths, in such a way that the ultrasonic beams remain collimated in the whole area under inspection. The final measurement arrays devices were manufactured at the Krautkramer company.

Figure 2 shows the disposition of the bi-plane array arrangement and the general scheme in relation to the inspection planning depicted in Figure 1, including the location of an isolate reflector (a hole in a plastic piece) with essential details of electronics and data acquisition requirements.

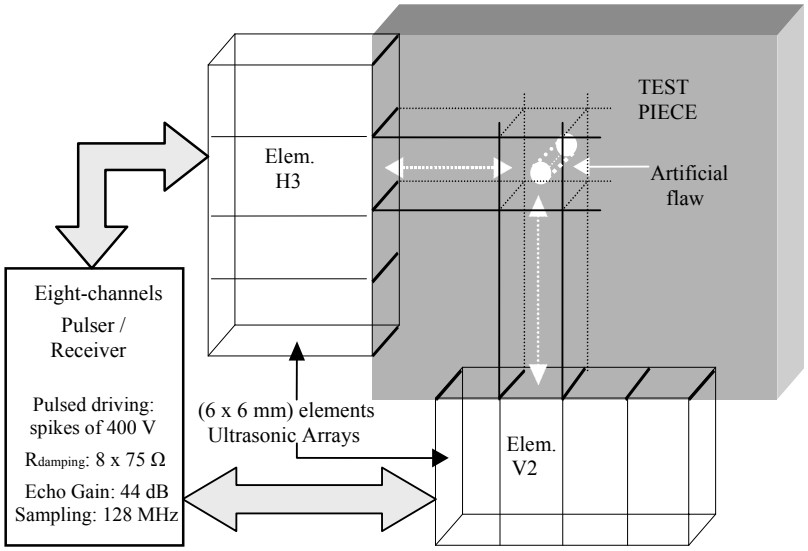

Figure 2. A block diagram of the multichannel ultrasonic prototype employed for the experiments (including 2 pulsed piezoelectric arrays).

Figure 3 shows the ultrasonic set-up arranged for orthogonal echo-signal acquisition. This right-angle device was especially developed for properly coupling and manually controlling both arrays, in order to inspect internal flaws in the edges or corners of the test pieces, which is a typically difficult problem where state-of-the-art of the robotic testing tools is currently inefficient.

Each elemental transducer was electrically driven with the high-voltage spikes, in a sequential way, for successive ultrasonic transmission cycles, and also was sequentially selected for echo acquisition. Here, we are concerned with near field radiations, and only one transducer emits / receives at the same time in the multichannel measurement. Thus, among all the echoes produced by the isolated reflector in response to the transducers shots, only those received in the two transducers located in line with the reflector (i.e., at their perpendicular projections on the horizontal and vertical apertures) will be captured, because during each transducer shot, the echoes acquisitions is electronically cancelled in the other transducers of the two arrays.

Additionally, these two transducers, in line with the reflector, may be susceptible to acoustic noise that depends on the internal structure of the material under inspection, and there is also the possibility

of electromagnetic interference. Under these conditions, the rest of the transducers of the two array apertures may measure noise but will not acquire echoes from the reflector hole. In the hole disposition shown in Figure 1, the pulsed echoes from the discontinuities in the piece material due to the reflector presence (plastic-air interface, in this case) will be received by transducers H3 and V2.

The arrival times of these echoes are determined by the distances from the reflector discontinuity to both transducers and the sound propagation velocity in the sample. The ultrasonic echo-traces received by transducers H1, H2, H4, V1, V3 and V4 will not contain any reflections from the internal hole.

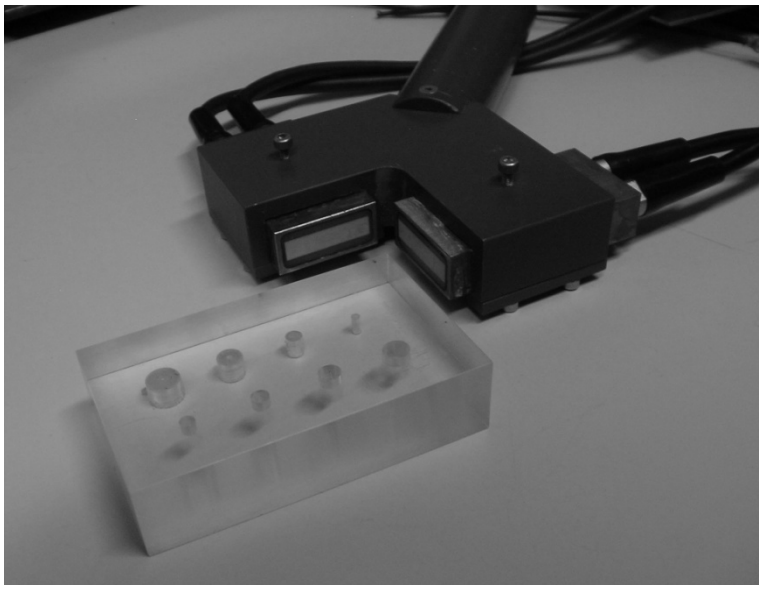

Figure 3. The experimental ultrasonic set-up (biplanar multi-element) based on two transducers arrays, Krautkramer KK - Refer. Z4RM6x6/4XE.

3. Wavelet transform considerations for pulsed ultrasonic traces

Finding an adequate representation of the signals in order to facilitate their processing is, in general, an ongoing problem whose possible solutions differ depending on the processing objective. The two most common signal representations are: a) in the time domain, which is very useful in the context of this work, related to internal NDI measurements in pieces, because the spatial localization of possible defects or flaws into a piece is closely related to the time in which the ultrasonic echoes appear; b) in the frequency domain, which is less commonly used in this type of ultrasonic applications, because in principle it does not permit deduce a spatial localization. The use of more complex time-frequency-scale representations (Cohen 1995, Hlawatsch and Boudreaux-Barlets 1992) for ultrasonic signals makes it possible to introduce spectral information into these applications, without loosing the spatial reference. This allows the variation with time of the frequency distribution of ultrasonic echo-signals to be shown in a 2D format. The two best known linear time-frequency representations are the Short-Time Fourier transform and the Wavelet transform. Both types can be easily implemented by means of linear filter banks. The wavelet transform is used here, and this point is now discussed.

The continuous wavelet transform of a signal $x(t)$ is defined as (Daubechies 1992):

$$WT_{x(t)}(\tau, a) = \int_{-\infty}^{\infty} x(t)\, \psi_{\tau,a}(t)\, dt \tag{1}$$

The signal $x(t)$ is expanded in terms of scaling and translations of a single prototype function $\psi(t)$ called mother wavelet.

$$\psi_{\tau,a}(t) = \frac{1}{\sqrt{|a|}} \psi\left(\frac{t-\tau}{a}\right) \tag{2}$$

where τ *is* the shift parameter and a the scale parameter; ($a, \tau \in R, a \neq 0$).

For practical implementation, both parameters are usually discrized:

$$a = a_0^j \qquad \tau = n a_0^j\, \tau_0 \tag{3}$$

where j and n are integers. In the most usual case, the dyadic case, the previous parameters take the values $a_0 = 2$, $\tau_0 = 1$, resulting the dyadic Discrete Wavelet Transform (DWT):

$$DWT_x(j,n) = \int_{-\infty}^{\infty} x(t) \frac{1}{\sqrt{2^j}} \psi\left(\frac{t}{2^j} - n\right) dt \qquad j, n \in Z \tag{4}$$

This transform can be easily computed using the algorithm of Mallat (Mallat 1989) which consists of a digital filter bank tree combined with decimation blocks. In the implementation of the wavelet transform, the input signal is passed through the linear filter banks, and the resulting outputs are taken as the inputs of the new stage. The iterative filtering process is only performed on the output of the low-pass filter; the partition of the signal spectrum provided by this transform is fixed: with narrow bands for low frequencies and broad bands for high frequencies. Due to downsampling, the number of coefficients at each decomposition scale is half the number at the previous scale.

Wavelet Packets Transform provides a great deal of flexibility in the spectrum decomposition that can be controlled and modified according to the particular analyzed ultrasonic signal. The iterative filtering process can be performed both on the output of the low-pass and on the high pass filter; the partition of the signal spectrum provided by this transform is flexible and can be adapted to the signal characteristics.

In the previous discrete transforms, the decimation in time or downsampling is applied to each frequency band in an individual way, thus time synchronization among different frequency bands may be complicated.

The Undecimated Wavelet Transform (UWT) is a special type of wavelet in which the time information is maintained in all the frequency bands during the decomposition. UWT is also a discrete approximation to the CWT that can be obtained from the following sampling of the CWT:

$$UWT_x(j,n) = \int_{-\infty}^{\infty} x(t) \frac{1}{\sqrt{2^j}} \psi\left(\frac{t-n}{2^j}\right) dt \qquad j,n \in Z \tag{5}$$

The most frequent implementation of the UWT transform is based on the *a'trous* algorithm which is similar to Mallat algorithm except that the signal is not downsampled and instead the filters are upsampled at each level of decomposition. Additionally, this is a redundant transform which is useful for structural noise reduction (Pardo et al 2008).

The conjunction of the undecimated wavelets and the wavelet packets gives rise to the Undecimated Wavelet Packet Transform (UWPT), which allows a decomposition of signal without frequency restrictions, while maintaining common time synchronization for all the bands. For these two reasons, the UWPT was the tool applied during our fusing process.

4. Fusing of pulse-echo pulse ultrasonic traces by 2D multiplicative UWPT processing

4.1. Description of the method.

The fusing process begins with the acquisition of the echo-pulses from the ultrasonic transducers in the two perpendicular arrays to obtain one A-scan register from each transducer. This results in 2*N* registers that need to be fused, where *N* is the number of transducers in each array. The UWPT of each ultrasonic echo-trace is obtained, and then the *L* frequency bands with the highest mean energy are selected in each trace. The trace bands are determined as a function of the frequency response of the array transducers and are previously fixed. The *L* time-domain signals corresponding to each selected band are the inputs of a new processing step. Thus, at this point, there are 2*NL* registers to be processed. Each register can be expressed as:

$$X_I(band,t) \tag{6}$$

where *X* can be V or H (vertical or horizontal), *I* is the transducer number (1…*N*), *band* is the band number (1…*L*), and *t* is time.

The next step is the matching of the information contained in each pair of perpendicular transducers associated to a same elemental inspected area. This matching could be the same for all the frequency range of the same ultrasonic trace due to the time synchronization property of the undecimated wavelet. If we suppose that the origin, point (0,0), is in the corner formed by transducers H1 and V1 in figure 1, then the matched pair for any inspected point (*x*,*y*) will be:

$$\left(H_{I1}(band,\frac{2x}{c}),V_{I2}(band,\frac{2y}{c})\right) \tag{7}$$

where, H_{I1} and V_{I2} are the transducers corresponding to each elemental area and *c* is the ultrasonic propagation velocity. Thus, the matching is made in function of the respective times of flight.

The different pairs of ultrasonic traces corresponding precisely to the same elemental inspection area (i.e. coming from two perpendicular transducers and having crossed projections over this zone)

configure the distinct elemental areas. The number of these areas is the product of the horizontal and vertical transducers number, in our case: N^2.

In order to reduce the problems caused by imperfect synchronization of the two matched pulses, the signal envelopes are previously calculated, since they are less sensitive to time-matching errors than the RF signals. These pulse envelopes are obtained by means of Hilbert transforms.

Next, one frequency band of each transducer signal is picked for the combination. Here, the same band is used for all the transducers, but it would also be possible to select a different band in each transducer. Thus, the full combination is made by dividing the whole process in several single band processes. Then, the task is divided into L combinations in time, and L 2D displays will be produced, one for each frequency band. Each single-band 2D representation is obtained using the time-domain combination method that used a 2D product (Rodríguez et al 2004).

$$2\text{D\_representation\_}band_i(x,y) = H_{I1}(band_i, \frac{2x}{c}) \bullet V_{I2}(band_i, \frac{2y}{c}) \tag{8}$$

Where, $band_i$ is the chosen band in each case.

Hence, we have L 2D representations, one for each band. The final step is the fusion of these L 2D displays by using a point-to-point product of them.

$$\text{Final\_2D\_representation}(x,y) = \prod_{i=1}^{L} 2\text{D\_representation\_}band_i(x,y) \tag{9}$$

It should be noted that, as the multiplicative type of fusing operators were chosen, it is not necessary to imperatively work with the RF signals, unlike as it happens in the case of traditional array additive focusing operations (Ramos and San Emeterio 2008).

A schematic diagram of the overall fusing technique is presented in Figure 4, where the different blocks that compound the processing method, together with their inputs and outputs, are shown.

4.2. The fusing quality index.

In order to measure the quality of the results of this wavelet fusing technique, and compare them with those obtained from previous techniques, we specify two parameters: SNR_{ini} and SNR_{2D} .

a) SNR_{ini} is defined as the SNR of initial ultrasonic traces acquired by each transducer. Mathematically, it is expressed by (Rodríguez et al 2004):

$$SNR_{ini}(dB) = 10\log\frac{\frac{1}{M}\sum_{i=1}^{M}(p(i))^2}{\frac{1}{K}\sum_{i=1}^{K}(n(i))^2} \tag{10}$$

where, p denotes the echo-pulse and n represents the noise signal; M and K are the length of the echo and of the whole ultrasonic trace, respectively.

b) SNR_{2D} is defined as the SNR of the final 2D representation after the fussing process. It can be mathematically expressed by (Rodríguez et al 2004):

$$SNR_{2D}(dB) = 10\log\frac{\frac{1}{M^2}\sum_{i=1}^{M}\sum_{j=1}^{M}(p_{2D}(i,j))^2}{\frac{1}{K^2}\sum_{i=1}^{K}\sum_{j=1}^{K}(n_{2D}(i,j))^2} \tag{11}$$

where, p_{2D} and n_{2D} denote the 2D representation of the 2D echo-information and of their noise content associated; M and K are the dimensions of the 2D rectangular representations, corresponding to the multipoint pulsed echoes and the whole ultrasonic information obtained from the elemental area considered.

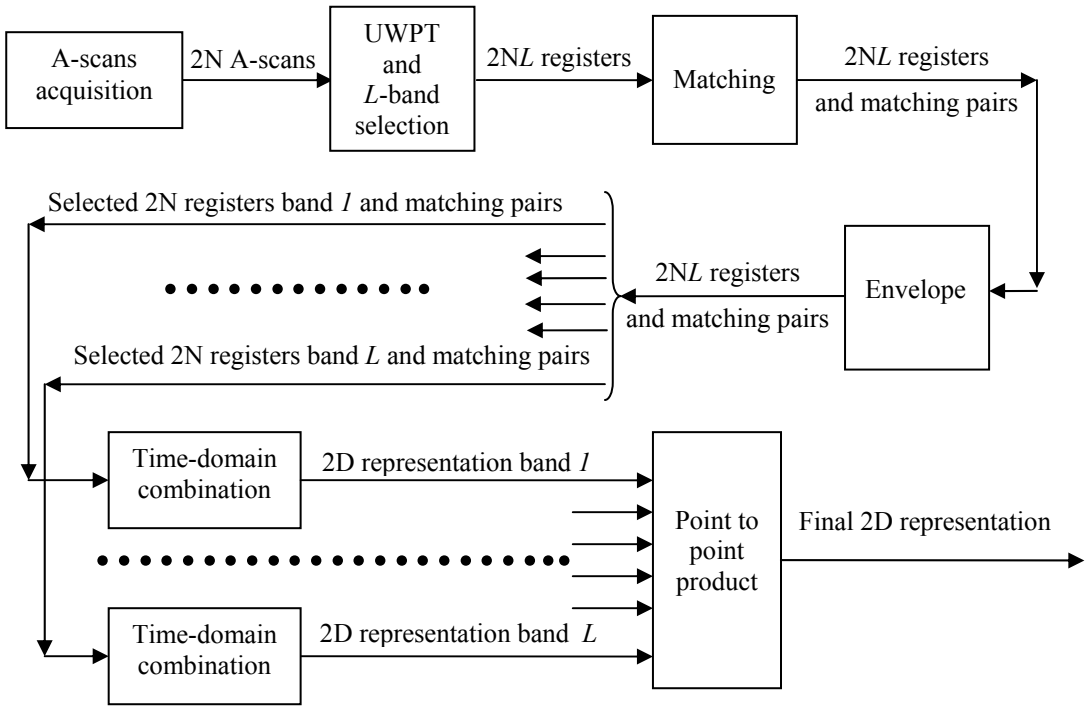

Figure 4. The functional scheme for echo-trace fusing using the UWPT method.

In the undecimated wavelet case, the combination process for each frequency band is similar to the basic time combination case described in (Rodríguez et al 2004). For the time combination method, the following expression was obtained:

$$SNR_{2Dtime}(dB) = 2 \cdot SNR_{ini}(dB) \tag{12}$$

The SNR of the 2D representation for each individual band, $SNR_{2D\_UWPT}^{(band-i)}$ is given by:

$$SNR_{2D\_UWPT}^{(band-i)}(dB) = 2 \cdot SNR_{ini}(dB) \tag{13}$$

The final approximate SNR, after the 2D product of all the 2D displays corresponding to the L frequency bands, SNR_{2D_UWPT} have been calculated by assuming that the 2D representations for each band are independent and perfectly synchronized (Rodríguez et al 2004b). Then SNR_{2D_UWPT} could be obtained by:

$$SNR_{2D\_UWPT} = \prod_{i=1}^{L} \frac{power\_pulse\_band\_i}{power\_noise\_band\_i} \tag{14}$$

The equation (14) can be expressed in dB as:

$$SNR_{2D\_UWPT}(dB) = \sum_{i=1}^{L} SNR_{2D\_UWPT}^{(band-i)} \quad (dB) \tag{15}$$

and combining expression (13) and (15) results

$$SNR_{2D\_UWPT}(dB) = 2 \cdot L \cdot SNR_{ini} \ \ (dB) \tag{16}$$

Consequently, in this case, the resulting SNR_{2D_UWPT} , measured in dB, presents a significant improvement over the SNR_{ini} , of one order of magnitude equal to two times the number of frequency bands used during the wavelet processing. Selected bands should be limited to the most significant ones. Including more frequency bands of lower energy will not improve the performance.

5. Flaw-detection results using the wavelet 2D fusing technique

The performance of the proposed wavelet fusing technique has been evaluated by means of the processing of: a) synthetic echo-trace registers and b) experimental ultrasonic echoes. In both cases, a rectangular piece with an artificial flaw (a small hole) was scanned by the 8 transducers comprising of the two ultrasonic arrays described above and that are located at different perpendicular planes.

5.1. Benchmark based on synthetic ultrasonic echo-traces

Synthetic ultrasonic traces simulating echoes from a small reflector were generated by inserting an experimental pulse-echo signal into synthetic coherent ultrasonic noise registers. The experimental ultrasonic echo was acquired from a methacrylate sample containing an isolated-flaw (a drilled hole), using for the measures a lightly-backed 5 MHz Krautkramer transducer. The coherent (grain-noise) registers (Gustafsson and Stepinski 1997, Lazaro et al 2002) were generated by initially processing white noise signals (randomly generated) with a digital filter having a spectrum equal to that of the experimental echo signal. Finally, the complete synthetic traces were obtained by adding the experimentally acquired pulse-echo signal to the synthetic noise registers. The noise content was unit-power normalized, whereas the echo-signal was multiplied by a constant with the aim of obtaining the different levels in SNR_{ini}.

The synthetic ultrasonic traces corresponding to transducers that do not receive echoes from the small reflector are composed exclusively of unit power normalized noise.

The length of the overall ultrasonic traces was 360 points (corresponding to 18 microseconds with a sampling frequency of 20 MHz), whereas the length of the echo-signals contained in these traces was of 18 samples. It should be noted that 18 microseconds is the total time of flight from (24 +24) mm (test piece depth), assuming a propagation velocity of 2667 m/s. Several sets of synthetic ultrasonic traces were generated with 10 different SNR_{ini} (0, 1, 2, 3, 4, 5, 6, 7, 8, 9 and 10 dB).

Table 1 shows the SNR_{2D_UWPT} results for the different sets of synthetic ultrasonic traces. First, the theoretical values for SNR_{2D_UWPT} obtained from equation (16) are given. Next, the mean values of SNR_{2D_UWPT} obtained from 10.000 synthetic ultrasonic traces and generated for each value of SNR_{ini}, are shown. Three different cases are presented, each using a different number of frequency bands [parameter L in expression (16)]. When applying the UWPT, the mother wavelet Daubechies 4 was used in all the cases.

The theoretical (corresponding to eq. 16) and the computed mean values of SNR_{2D_UWPT} (obtained for 2, 3 and 4 frequency bands) show very good agreement. The improvements in the results of SNR_{2D_UWPT} , by a factor $2L$ as predicted in (16), are also clearly confirmed. This represents a significant improvement with respect to SNR_{ini} in the real echo information, of approximately 800% (in dB) when using four bands in the wavelet processing.

SNR_{ini} (dB)	SNR_{2D_UWPT}(dB)					
	L = 2 bands		L = 3 bands		L = 4 bands	
	(a)	(b)	(a)	(b)	(a)	(b)
0	0	0.4	0	0.0	0	1.0
1	4	3.5	6	5.7	8	8.7
2	8	7.4	12	11.6	16	16.6
3	12	11.4	18	17.4	24	24.5
4	16	15.4	24	23.4	32	32.5
5	20	19.4	30	29.3	40	40.4
6	24	23.3	36	35.2	48	48.4
7	28	27.3	42	41.2	56	56.3
8	32	31.3	48	47.2	64	64.3
9	36	35.3	54	53.2	72	72.3
10	40	39.3	60	59.1	80	80.3

Table 1. The values of SNR for the 2D representations obtained using the UWPT fusing method. (a) Theoretical values from Eq. (16); (b) Computed mean value from 10000 synthetic traces in each value of SNR_{ini}

Figure 5.b and 5.c show computed 2D displays for the overall inspected sample (having 16 small internal cells as in the scheme of Figure 1). The correct localization of an isolated punctual flaw can be clearly appreciated, in spite of being an unfavorable case due to the severe SNR value of the simulated traces. Figure 5.a shows the initial A-scans corresponding to the eight H-V transducers with SNR_{ini} = 3 dB, where it can be observed that the echo produced by the hole cannot be accurately located in time.

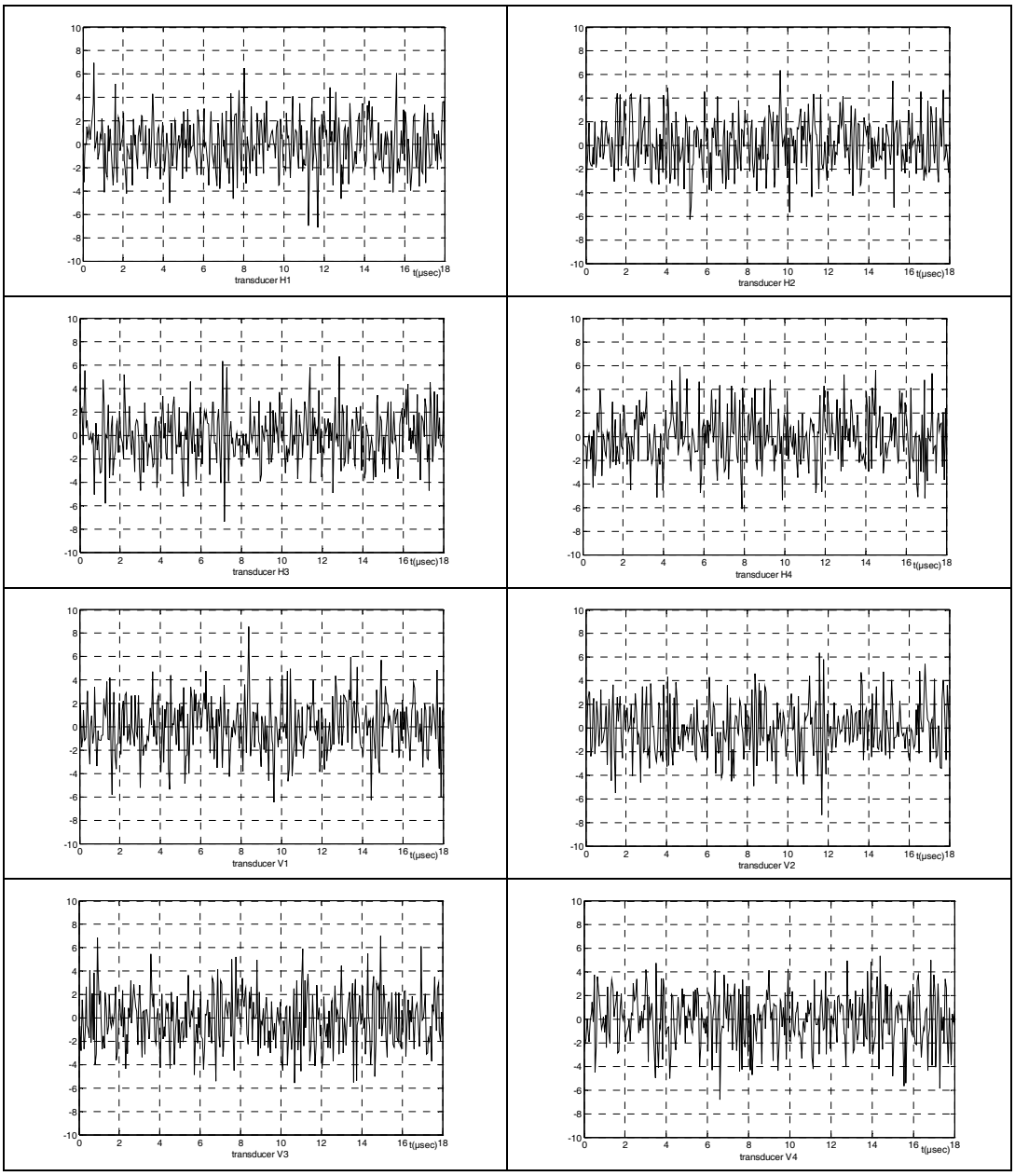

a)

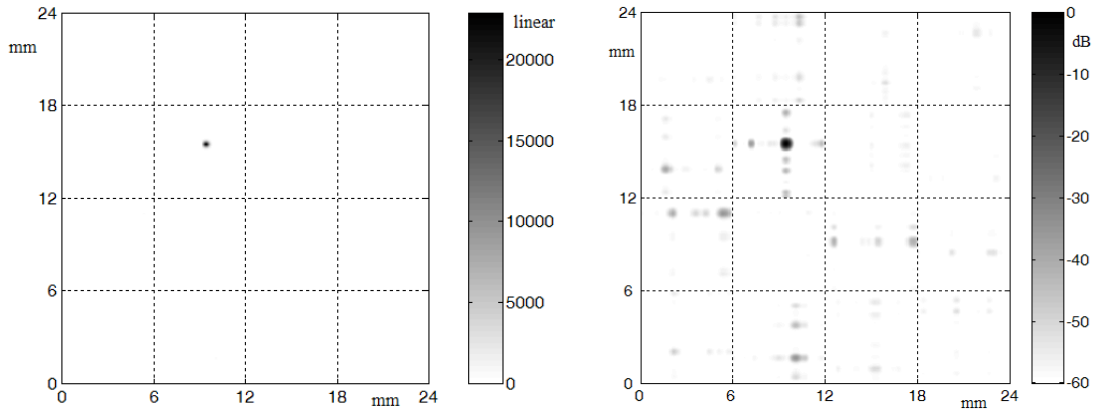

b) c)

Figure 5. The 2D location of a punctual flaw obtained using the wavelet fusing method. (a) Initial synthetic traces from 8 transducers with SNR_{ini} = 3 dB. (b) and (c) 2D flaw location displays for the overall test piece (16 cells, 24 x 24 mm), using linear and logarithmic scales, respectively.

The noise contained in these initial traces was composed of both white noise (modeling "thermal" noise commonly induced by electronic instrumentation) and coherent noise (modeling "grain" noise intrinsic to the inner texture of some materials under inspection, like composites or special steels for example). The noise power percentages were 66% and 33 % respectively.

The echo-pulses from the H3 and V2 transducers can be identified with difficulty, immersed in the noise, beginning at around 6.7 and 11.2 microseconds in the respective traces shown in Figure 5.a. In addition, there are other numerous echo-signals that could be interpreted as being associated to other possible material flaws. In this case, two frequency bands have been used for the wavelet based fusing method. In the resulting detection displays of Figures 5.b-c, good location of the flaw as well as an important reduction of noise can be appreciated from both linear and logarithmic scaled graphs.

The good reflector location is related to the data size of these 2D representations of the inspected area, which is 360x360 (129600) dots, corresponding to the 24 x 24 mm overall test piece section. Thus, from 2880 initial data points (360 per transducer), a 2D display with 129600 points was obtained for the whole inspected area by means of the fusing processing proposed here.

The 2D fusing method proposed in the paper not only obtains a better SNR but also a resolution improvement. The theoretical numerical quantification of this resolution in pixels is easy to obtain and has been already treated in a previous work (Rodríguez et al 2007a). The more interesting final acoustic resolution in emission-reception (in mm) has a much more difficult quantification depending of many factors as ultrasonic time-width & bandwidth of the emitted pulse, sampling frequency or diffraction effects. In any case, it would be a complex pending task for a possible future work extending the current paper technique.

5.2. Benchmark based on experimental ultrasonic echoes

The experimental ultrasonic echo-traces were acquired from a methacrylate sample having a drilled 2 mm cylindrical hole, by using the multi-channel prototype described in section 2. The inspected area size is again 24x24 mm (Fig. 2). During echo-acquisition, ultrasonic arrays were coupled to the sample with coupling gel, ensuring that transducers H3 and V2 remain located in line with the cylindrical hole.

A set of ultrasonic echo-traces, acquired with the ultrasonic set-up of Figure 3, was processed using the UWPT technique. In this case, the initial traces had a low level of material noise, because they were acquired from a mainly homogeneous sample with very low acoustic attenuation and scattering. The A-scans registers from the receiver transducers active in this case, H3 and V2, are shown in figure 6, where only values corresponding to possible echo-signals from the hole are displayed. In fact, the remaining A-scans from the transducers (H1, H2, H4, V1, V3 and V4) are almost zero in amplitude.

2D fused displays for the location of this hole, obtained with our wavelet fusing procedure, are presented in figure 7, using both linear and logarithmic scales. The real hole contour is shown in figure 7 with a circle of 2 mm in diameter. Very good accuracy (of sub-millimeter order) in the location of the hole contour related to its nearest zone to the involved transducers (H3 and V2) can be appreciated.

The measurement procedure presented here is for punctual defects. In real experiments we are using a "perfectly drilled" hole (containing air) with diameter equal to 2 mm. Thus, we are detecting the reflecting points of the circumference (by density discontinuity) with minimum distance to vertical and horizontal transducers.

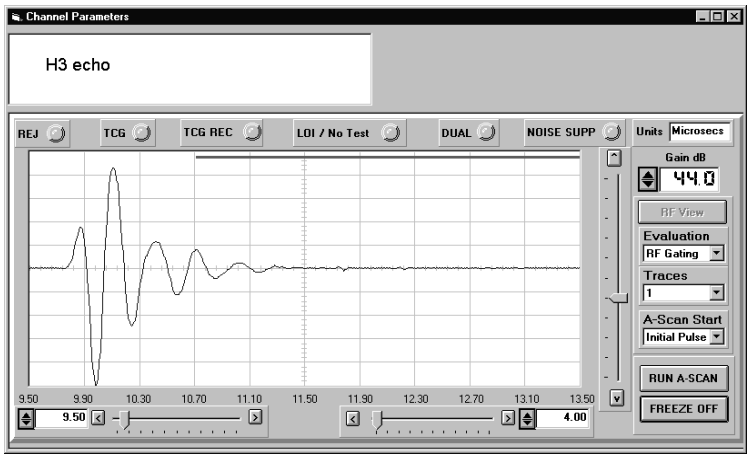

a)

b)

Figure 6. The A-scans from transducers H3 (a) and V2 (b) using the experimental setup shown in figures 2 and 3.

Due to the extent of the logarithmic scale (60 dB) employed in these displays, small contour distortions and co-lateral secondary detection indications, associated to the fusing method, can be easily observed and quantified. In figure 7 a zoom of only one elemental area (6 x 6 mm) is represented, at difference of the whole piece area (24 x 24 mm) shown in figures 5. b-c. This small area (36 mm^2) corresponds to the small intersection zone "illuminated" by the transducers H3 & V2 that are aligned with the hole. This zoom helps to calibrate, with accuracy, the spatial resolutions in these figures.

In relation to processing parameters selected for this detection case, the mother wavelet Daubechies 4 was used in the UWPT, as in the case of synthetic echoes (5.1), but only with L= 2 bands.

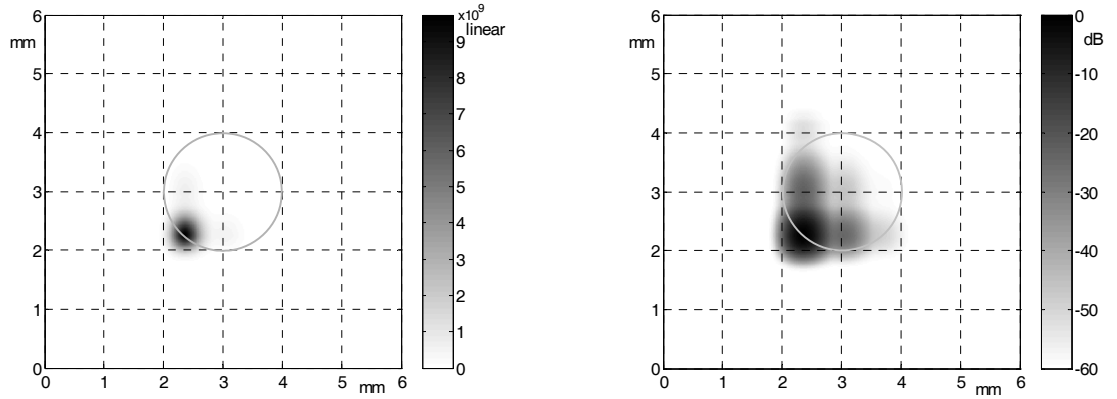

Figure 7. 2D displays of the inspection results from the H3-V2 intersection elemental cell (6x6 mm) of the methacrylate sample containing a 2mm circular hole, after processing the experimental traces using the UWPT fusing method. Zooms of the cell inspection using: (a) linear and (b) logarithmic scales.

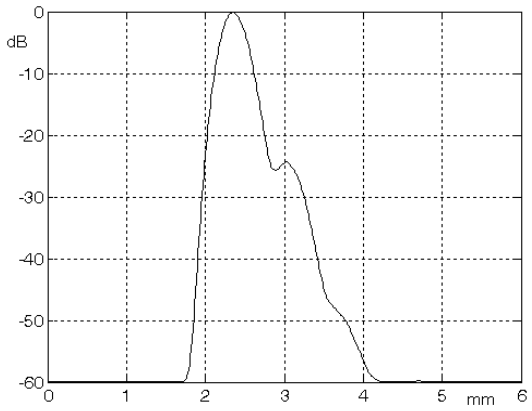

Figure 8. 1D profile of a horizontal cross-section in figure 7.b at a height of 2.3 mm (the maximum value line in 2D display). A small lateral "lobe" at a distance of 0.7 mm from the peak can be appreciated.

Figure 8 shows a 1D horizontal "cut" performed at a distance of 2.3 mm in a vertical direction of the logarithmic-scaled plot in figure 7.b, where a narrow main lobe merged with two smaller secondary perturbations can be seen. This vertical distance corresponds to the point where the maximum value in the 2D echo-fusing display was registered, which is slightly displaced (0.3 mm) from the borders of the hole. This displacement is mainly due to the spatial translation of the small rise-time in the envelope of the ultrasonic pulses emitted by the broadband array transducers used here for the experiments. This 1D profile confirms the good localization capability of the hole contour, available using the 2D wavelet-based fusing method.

6. Results discussion and comparative evaluation with other similar combination procedures.

In this section, the results presented in the previous paragraphs will be validated by comparing them with results obtained from the application of other two similar techniques (previously proposed also for flaw detection with the same perpendicular-array ultrasonic disposition): 1) direct time-domain (Rodríguez et al 2004) and 2) time-domain Wigner-Ville based (Rodríguez 2003) combination techniques. The same synthetic and experimental benchmarks used in section 5 will be employed in this complementary evaluation.

6.1. Comparative evaluation using synthetic registers.

For the evaluation with synthetic echo-traces, the comparative valuation index is based on the SNR improvement. Table 2 shows the SNR_{2Dtime} results for the direct time-domain combination technique using different sets of synthetic ultrasonic traces with different mean values of SNR_{ini}, as used in Table 1. The SNR_{2Dtime} values obtained from equation (12) and the SNR_{2Dtime} mean values obtained using 10000 synthetic ultrasonic traces are given.

Table 3 shows the results for SNR_{2D_Wigner} using the Wigner-Ville based time-combination technique, where three different cases have been calculated using distinct number of frequency bands. The computed values of SNR_{2D_Wigner} are obtained from mean values after processing 10000 synthetic ultrasonic traces, and the theoretical results are calculated from the following expression (Rodríguez 2003):

$$SNR_{2D\_Wigner}(dB) \cong 3 \cdot L \cdot SNR_{ini} \quad (dB) \tag{17}$$

It can be appreciated that the wavelet based fusing technique performs approximately L times better than the direct time domain combination technique with respect to the SNR improvement. On the other hand, the wavelet based fusing technique shows a worse performance than the Wigner-Ville technique in this particular aspect, but the wavelet technique has two interesting advantages:
a) it maintains linearity during the fusing, and b) it has a lower computational cost. These advantages compensate for the slightly reduced value in the SNR of the fused orthogonal echo signals.

Simulations comparing computational costs have been done using Matlab. Results show that the process time of UWPT technique is about 0.7 the associated to the WVT procedure. In these simulations the UWPT was implemented by means of filter banks calculating the outputs for all possible frequency bands. In a real case, after calibration, only the bands used in combination process should be computed reducing the computational cost. The WVT was implemented with the algorithm of (Boashash and Black 1987). Both UWPT and WVT were calculated with the same frequency resolution.

SNR_{ini} (dB)	SNR_{2Dtime}(dB)	
	(a)	**(b)**
0	0	0.2
1	2	2.2
2	4	4.2
3	6	6.2
4	8	8.1
5	10	10.1
6	12	12.1
7	14	14.1
8	16	16.1
9	18	18.1
10	20	20.1

Table 2. The values of SNR in the 2D representations obtained by the direct time-domain combination method. (a) The theoretical values from Eq. (12); (b) The computed mean values using 10000 synthetic traces.

SNR_{ini} (dB)	SNR_{2D_Wigner} (dB)					
	2 bands		**3 bands**		**4 bands**	
	(a)	**(b)**	**(a)**	**(b)**	**(a)**	**(b)**
0	0	5.0	0	8.6	0	12.9
1	6	8.9	9	12.8	12	18.1
2	12	11.9	18	19.0	24	25.3
3	18	16.8	27	28.0	36	38.9
4	24	21.6	36	35.7	48	50.4
5	30	27.6	45	45.3	60	64.3
6	36	34.6	54	56.1	72	80.9
7	42	41.5	63	63.2	84	94.7
8	48	48.9	72	78.5	96	111.3
9	54	56.9	81	90.7	108	127.9
10	60	64.2	90	101.7	120	142.0

Table 3. The values of SNR in the 2D representations obtained by the Wigner-Ville based combination method. (a) The theoretical values from Eq. (17); (b) The computed mean values using 10000 synthetic traces.

6.2. Comparative evaluation using experimental traces.

For analyzing the three distinct digital processes that combine the experimental orthogonal echoes, a comparative evaluation is performed using 2D displays obtained from the same set of measured ultrasonic traces. Figure 9 shows the 2D representation of the H3-V2 elemental area obtained by using the direct time combination technique, along with the same set of experimental traces of figure 7. In this figure, some distortion of the hole contour can be seen (which is more clearly visible in 9.b, with the logarithmic scale); there are shadow zones in the form of a cross that are more greatly extended than in Figure 7.b. But even when using this worst processing option, a reasonably accurate spatial location of the hole contour can still be obtained if the linear scale (Fig. 9.a) is used.

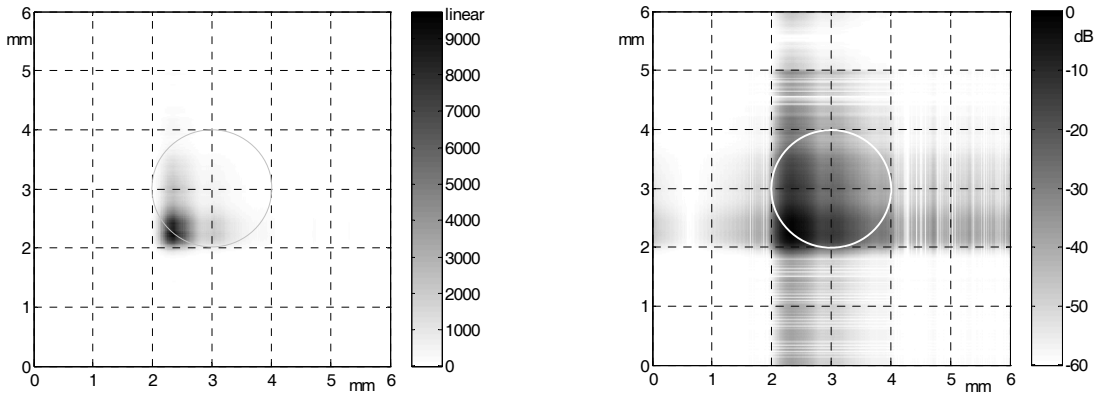

Figure 9. A zoom of the 2D representation of the H3-V2 elemental cell (6x6 mm) containing a 2 mm hole, using the direct time-domain combination method: with linear (a) and logarithmic (b) scales.

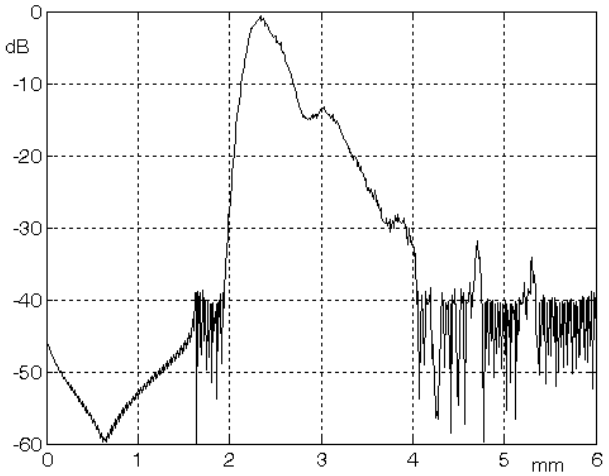

Figure 10. The 1D profile corresponding to the horizontal section taken from figure 9.b at a height of 2.3 mm (line of the maximum value in 2D display). A number of small lateral lobes (located between 3 and 6 mm) can be seen; the largest, at 3 mm, has a significant amplitude of -13dB.

Figure 10 shows (similarly to figure 8) a 1D horizontal cut of the logarithmic display in Figure 9.b, performed at a distance of 2.3 mm in a vertical direction. Here, the worst main and secondary detection lobes are found. In order to interpret these results, it should be noted that the border of the real hole starts at 2 mm in the horizontal direction and at 2 mm in the vertical direction, measured from the point (0,0) in H3-V2 elemental cell perimeter. Away from zone of the hole, indications of spurious detection appear in the 1D profile shown in figure 10 at around 3 mm to the right of the hole left side. However, these are reduced in magnitude by 30 dB respect to the maximum. Nevertheless, these spurious indications are not observed when using the wavelet option proposed in this paper.

This type of undesired distortions and secondary indications, appearing when these biplane detection methods are applied, would play a role similar to the well-known lateral and grating lobes in the conventional far-field uni-planar array focusing imaging when arrays are spatially under-sampled. But, in this biplane case, their acoustic near-field origins are quite different.

Finally, figure 11 shows the 2D representation of the H3-V2 elemental area obtained by using the Wigner-Ville combination technique, with the same set of experimental traces as in figure 7. Also, figure 12 depicts a horizontal cut performed at a distance of 2.3 mm as in figures 8 and 10.

Note that when using the wavelet-based fusing method proposed here, the first small lobe (with an amplitude of -25 dB in figure 8) associated with the secondary indications appears to be merged with the main lobe, whereas a similar lobe (with an amplitude of - 46dB) is obtained when using the Wigner Ville combination method, but is separated from the main lobe, as shown in figure 12.

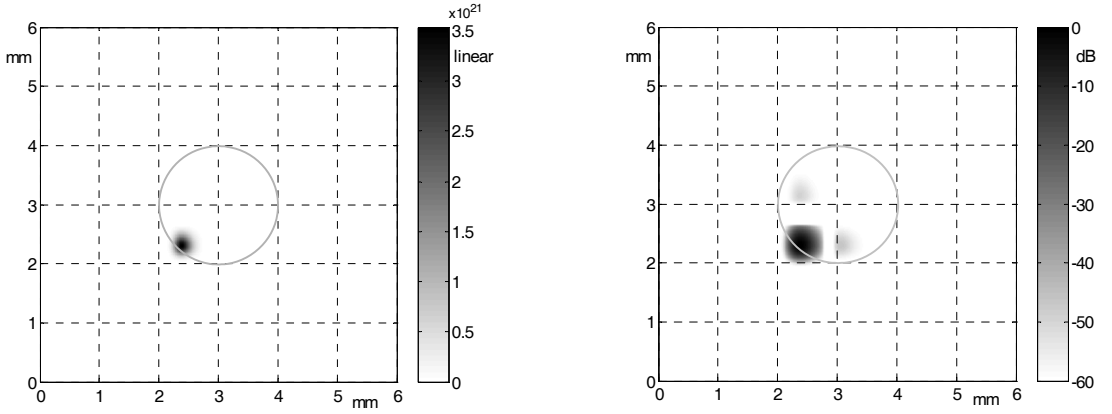

a) b)

Figure 11. A zoom of the H3-V2 elemental cell (6x6 mm) with a 2mm hole: location results as in Figures 7 and 9, but using the Wigner-Ville combination method, with linear (a) and logarithmic (b) scales.

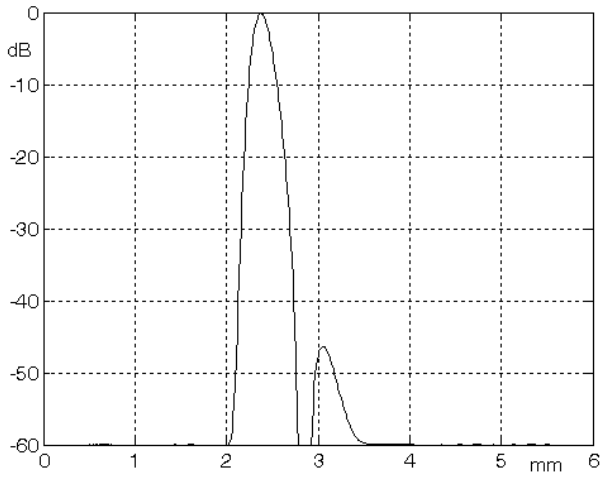

Figure 12. The 1D profile corresponding to a horizontal section of figure 11.b (with logarithmic scale), at a height of 2.3 mm (line of maximum value). A small lateral "lobe" separated from the main lobe is seen.

It is clear that these 1D profiles, that accurately describe the hole location, confirm the good flaw location provided by the two 2D combination methods based on 2-D transforms. The results achieved using the Wigner-Vile option present the "cleanest" result (in terms of SNR) although the wavelet transform option has a similar global performance.

The good results obtained from the laboratory benchmark experiments, show the ability of the wavelet fusing option when applied to isolated-flaw reflection patterns, in terms of the values of SNR obtained and of the potential bi-dimensional resolutions. This good basic performance can be extended to more complex real inspection situations with closely spaced flaws or with flaws located at the cells borders (i.e., with receiving irradiation by more than two beams). The viability of these alternative options has already been demonstrated in two preliminary works (Rodríguez et al 2005; Rodríguez et al 2007).

7. Conclusions.

A new low-cost processing technique for efficient fusing of ultrasonic echo-measures related to orthogonal-beams acquired from perpendicularly located NDI array transducers has been described and demonstrated. It introduces a digital signal processing procedure based on the UWPT transform combined with several 2D product operators. The technique provides precise location of isolated flaws even from noisy echoes and only requires a small number of transducers mounted in two perpendicular planes. A significant reduction of 800% (in dB) is achievable for the SNR in the final fused display.

Accurate two-dimensional displays for flaw location showing greatly improved 2D SNR were obtained using the wavelet trace fusing technique. Its good performance in flaw detection has been confirmed by means of the processing of eight simulated and eight measured ultrasonic echo-registers. A simple theoretical expression has been derived, accounting for the final SNR after the wavelet

technique application. Good accuracy has been shown by the agreement of calculation results with those obtained through synthetic and experimental benchmarks.

Results using two other previously proposed, but similar, combination methods (direct time domain and Wigner-Ville based) were calculated and plotted as both 2D displays and 1D profiles, using a large amplitude range of 60 dB; the secondary lobes related to these combination processes are clearly seen. A comparison of these results with those from the wavelet-based fusing method shows that this is clearly superior in performance to the direct-time combination technique, and that presents a similar performance than the Wigner-Ville transform option.

Finally, the wavelet-based fusing method does not have non-linear terms as does the Wigner-Ville option. This is a very important advantage as a low computational cost is required for implementation. The results presented in this paper allow future research to be suggested; for instance, the extension of the technique proposed to more complex inspection scenarios, with multiple and closely located flaws or for applying it to some real problems and geometries encountered at the borders and corners of industrial pieces in nuclear and aeronautic testing, where inspection with the usual robotic means are not capable of accessing to possible flaws located in the sides of the scans.

Acknowledgements

This work was supported by the National Plan of the Spanish Ministry of Science & Innovation (R&D Project DPI2008-05213).

References

Boashash B. and Black P J 1987 An efficient real-time implementation of the Wigner-Ville distribution *IEEE Trans. Acoustic, Speech and Signal Processing*, Vol 35, pp 1611-1618.

Castellanos L, Calás H and Ramos A 2010 Limited-diffraction wave generation by approaching theoretical x-wave electrical driving signals with rectangular pulses *Ultrasonics*, Vol 50, pp 116-121.

Chang Y F and Hsieh C I 2002 Time of flight diffraction imaging for double-probe technique *IEEE Trans. Ultrason. Ferroel, Freq. Cont.* vol 49(6) pp 776-783.

Cohen L 1995 *Time-Frequency Analysis* Prentice Hall PTR Englewood Cliffs New Jersey.

Daubechies I 1992 *Ten Lectures on Wavelets* Society for Industrial and Applied Mathematics PhiladelphiaPA

Defontaine M et al 2004 2D array device for calcaneus bone transmission: an alternative technological solution using crossed beam forming *Ultrasonics* vol 42 pp 745-752.

Engl G and Meier R 2002 Testing large aerospace CFRP components by ultrasonic multichannel conventional and phased array pulse-echo techniques *NDT.net*, vol 7 num 10.

Ullate L G, Ramos A and San Emeterio J L 1994 Analysis of the ultrasonic field radiated by time-delay cylindrically focused linear arrays *IEEE Trans. Ultrason. Ferroelec. Freq. Control* vol. 41 (5) pp. 749-760.

Gustafsson M G and Stepinski T 1997, Studies of split spectrum processing, optimal detection, and maximum likelihood amplitude estimation using a simple clutter model, *Ultrasonics* 35 pp. 31-52.

Hillger W, Ahrholdt M, Rohling H and Henrich R 2004 Non-contact ultrasonic imaging techniques for composites components *16th World Conference on NDT. Proceedings WCNDT2004* Montreal paper 656.

Hlawatsch F and Boudreaux-Barlets G 1992 Linear and Quadratic Time-Frequency Signal Representations *IEEE Signal Processing Magazine* vol 9(2) pp. 21-67.

Lazaro J C, San Emeterio J L, Ramos A and Fernandez-Marron J L 2002 Influence of thresholding procedures in ultrasonic grain noise reduction using wavelets *Ultrasonics* vol. 40 pp 263-267.

Lu J Y, Zou H and Greenleaf J F 1992 Experimental verification of nondiffracting X waves" *IEEE Trans. Ultrason., Ferroelect., and Freq. Contr.* vol 39 pp 441-446.

Mallat S 1989 A theory for multiresolution signal decomposition: the wavelet representation *IEEE Transaction on Pattern Analysis and Machine Intelligence* vol 11 pp 674-693.

Meyer A W and Candy J V 2002 Iterative Processing of Ultrasonic Measurements to Characterize Flaws in Critical Optical Components *IEEE Trans. on Ultrason. Ferroel. and Freq. Cont.* vol 8 pp 1124-1138.

Newhouse V L, Bilgutay N M, Saniie J and Furgason E S 1982 Flaw-to-grain echo enhancement by split-spectrum processing *Ultrasonics* vol 20 pp. 59-68

Pardo E, San Emeterio J L, Rodriguez M A and Ramos A 2008 Shift Invariant Wavelet Denoising of Ultrasonic Traces *Acta Acustica United with Acustica* vol 94 (5) pp 685-693.

Ramos A, Sanz P T and Montero F 1987 Broad-band driving of echographic arrays using 10ns-500 v efficient pulse generators *Ultrasonics* vol 25 pp. 221-228.

Ramos A, Montero F, Sanz P T, Torregrosa J M 1993 A 5 MHz high-voltage demultiplexed ultrasonic array system for rapid-scan testing of advanced materials *Sensor and Actuators A* 37-38, pp. 385-390

Ramos A and San Emeterio J L 2008 Ultrasonic systems for non-destructive testing using piezoelectric transducers. Electrical responses and main schemes *Chapt. 16 in book "Piezoelectric transducers and their Applications. Edit. Springer-Verlag*, pp. 413-431 ISBN 978-3-540-77507-2.

Reguieg D, Padilla F, Defontaine M, Patat F and Laugier P 2006 Ultrasonic transmission device based on crossed beam forming *Proc. of the 2006 IEEE Ultrasonic Symposium*, pp. 2108-2111

Rodríguez M A 2003 Ultrasonic non-destructive evaluation with spatial combination of Wigner-Ville transforms *NDT&E International* vol 36 pp. 441-445.

Rodríguez M A, Ramos A and San Emeterio J L 2004 Localization of isolated flaws by combination of noised signals detected from perpendicular transducers *NDT&E International* 37 pp. 345-352.

Rodríguez M A, San Emeterio J L, Lázaro J C and Ramos A 2004a Ultrasonic Flaw Detection in NDE of Highly Scattering Materials using Wavelet and Wigner-Ville Transform Processing *Ultrasonics* vol 42 pp 847-851.

Rodríguez M A, Ramos A, San Emeterio J L and Pérez J J 2004b Flaw location from perpendicular NDE transducers using the Wavelet packet transform *Proc. IEEE International Ultrasonics Symposium 2004* (*IEEE Catalog 05CH37716C*) pp 2318-2232.

Rodríguez M A, Ramos A and San Emeterio J L 2005 Multiple flaws location by means of NDE ultrasonic arrays placed at perpendicular planes *Proc. IEEE International Ultrasonics Symposium 2005* (*IEEE Catalog 0-7803-9383-X/05*) pp. 2074-2077.

Rodríguez M A, Ramos A and San Emeterio J L 2007 Ultrasonic inspection with two perpendicular arrays of multiple defects located in some critical dispositions *Proc. the International Congress on Ultrasonics 2007*, Paper ID 1280, pp. 1-4.

Rodríguez M A, Ramos A and San Emeterio J L 2007a Ultrasonic transduction system for imaging with a low number of transducers located at different planes. *Proc. The 19th International Congress on Acoustic 2007*(*special issue of the journal Revista de Acústica* vol 38), Paper ID ULT15-010, pp. 1-6.

Roy O, Mahaut S and Serre M 1999 Application of ultrasonic beam modeling to phased array testing of complex geometry components. *Review of Progress in Quantitative Non destructive Evaluation* Kluwer Acad. Plenum Publ. NewYork vol 18 pp. 2017-2024.

SNR_{ini} (dB)	SNR_{2D_UWPT}(dB)					
	***L* = 2 bands**		***L* = 3 bands**		***L* = 4 bands**	
	(a)	**(b)**	**(a)**	**(b)**	**(a)**	**(b)**
0	0	0.4	0	0.0	0	1.0
1	4	3.5	6	5.7	8	8.7
2	8	7.4	12	11.6	16	16.6
3	12	11.4	18	17.4	24	24.5
4	16	15.4	24	23.4	32	32.5
5	20	19.4	30	29.3	40	40.4
6	24	23.3	36	35.2	48	48.4
7	28	27.3	42	41.2	56	56.3
8	32	31.3	48	47.2	64	64.3
9	36	35.3	54	53.2	72	72.3
10	40	39.3	60	59.1	80	80.3

Table 1. The values of SNR for the 2D representations obtained using the UWPT fusing method. (a) Theoretical values from Eq. (16); (b) Computed mean value from 10000 synthetic traces in each value of SNR_{ini}

SNR_{ini} (dB)	SNR_{2Dtime}(dB)	
	(a)	**(b)**
0	0	0.2
1	2	2.2
2	4	4.2
3	6	6.2
4	8	8.1
5	10	10.1
6	12	12.1
7	14	14.1
8	16	16.1
9	18	18.1
10	20	20.1

Table 2. The values of SNR in the 2D representations obtained by the direct time-domain combination method. (a) The theoretical values from Eq. (12); (b) The computed mean values using 10000 synthetic traces.

SNR_{ini} (dB)	SNR_{2D_Wigner} (dB)					
	2 bands		**3 bands**		**4 bands**	
	(a)	**(b)**	**(a)**	**(b)**	**(a)**	**(b)**
0	0	5.0	0	8.6	0	12.9
1	6	8.9	9	12.8	12	18.1
2	12	11.9	18	19.0	24	25.3
3	18	16.8	27	28.0	36	38.9
4	24	21.6	36	35.7	48	50.4
5	30	27.6	45	45.3	60	64.3
6	36	34.6	54	56.1	72	80.9
7	42	41.5	63	63.2	84	94.7
8	48	48.9	72	78.5	96	111.3
9	54	56.9	81	90.7	108	127.9
10	60	64.2	90	101.7	120	142.0

Table 3. The values of SNR in the 2D representations obtained by the Wigner-Ville based combination method. (a) The theoretical values from Eq. (17); (b) The computed mean values using 10000 synthetic traces.

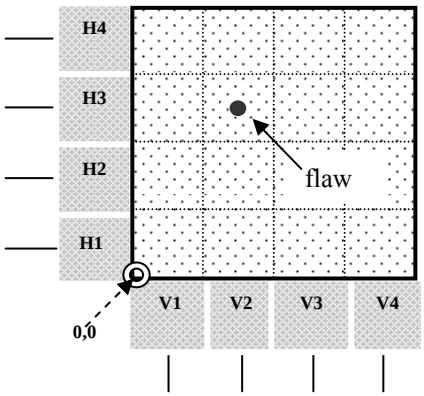

Figure 1. The geometry of the inspection configuration: detection of a single-flaw in a 2D arrangement using 8 transducers.

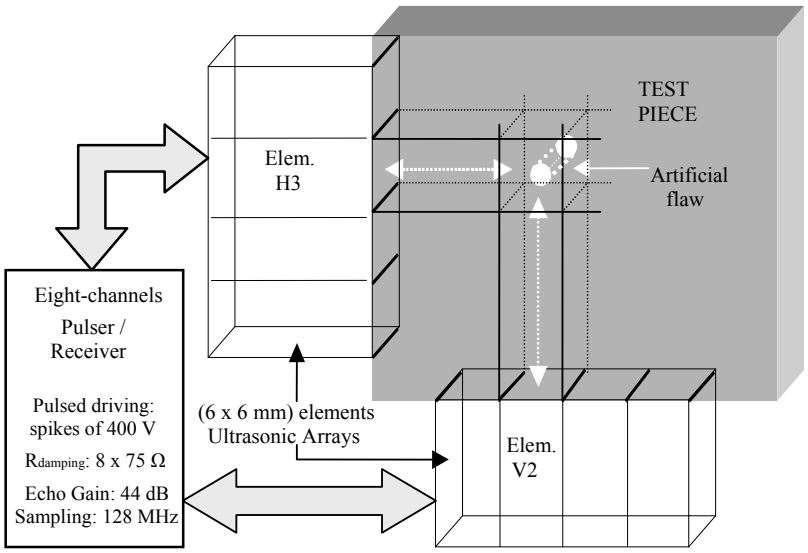

Figure 2. A block diagram of the multichannel ultrasonic prototype employed for the experiments (including 2 pulsed piezoelectric arrays).

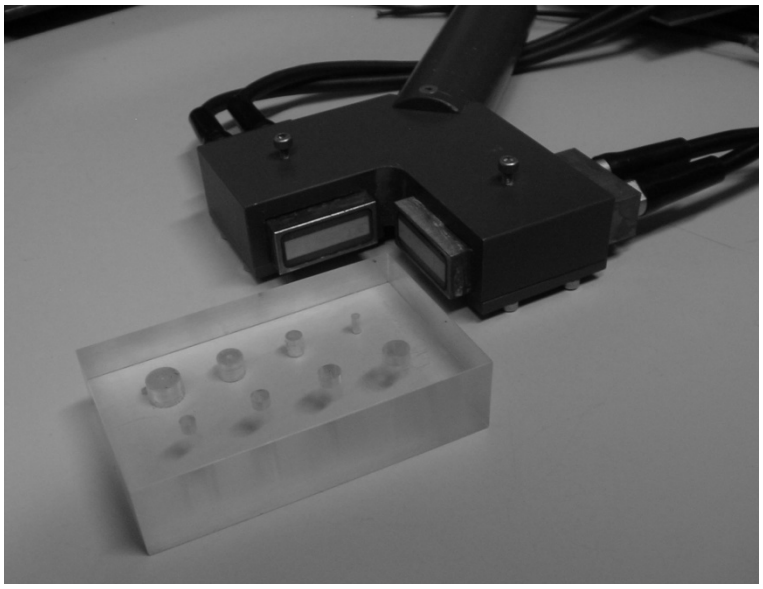

Figure 3. The experimental ultrasonic set-up (biplanar multi-element) based on two transducers arrays, Krautkramer KK - Refer. Z4RM6x6/4XE.

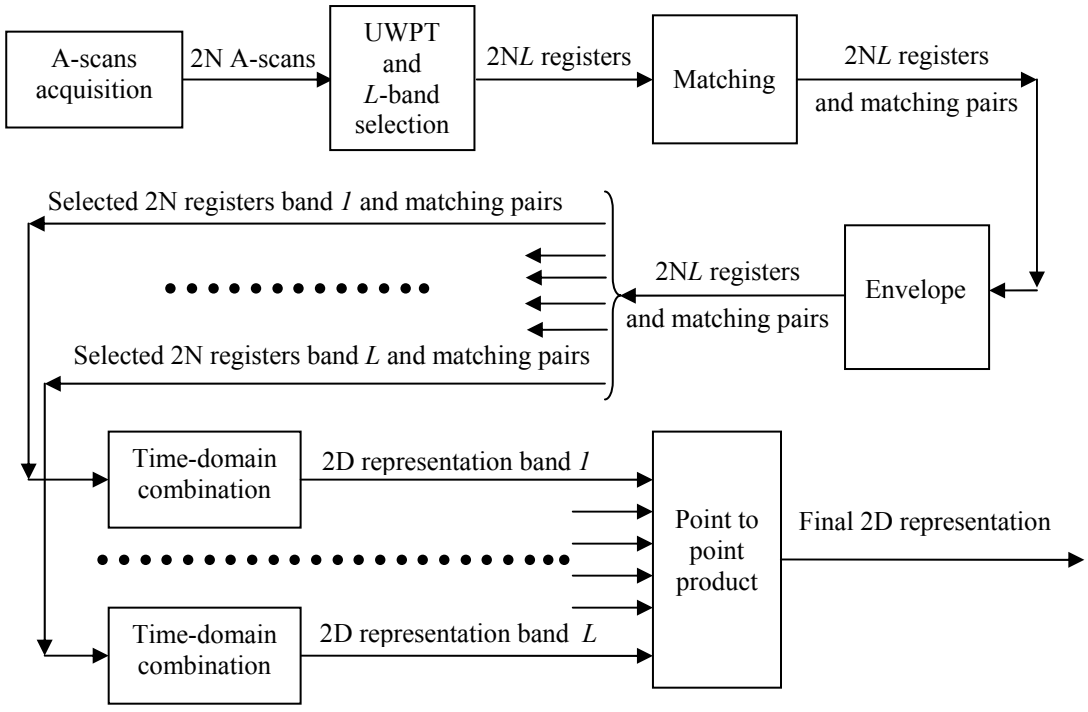

Figure 4. The functional scheme for echo-trace fusing using the UWPT method.

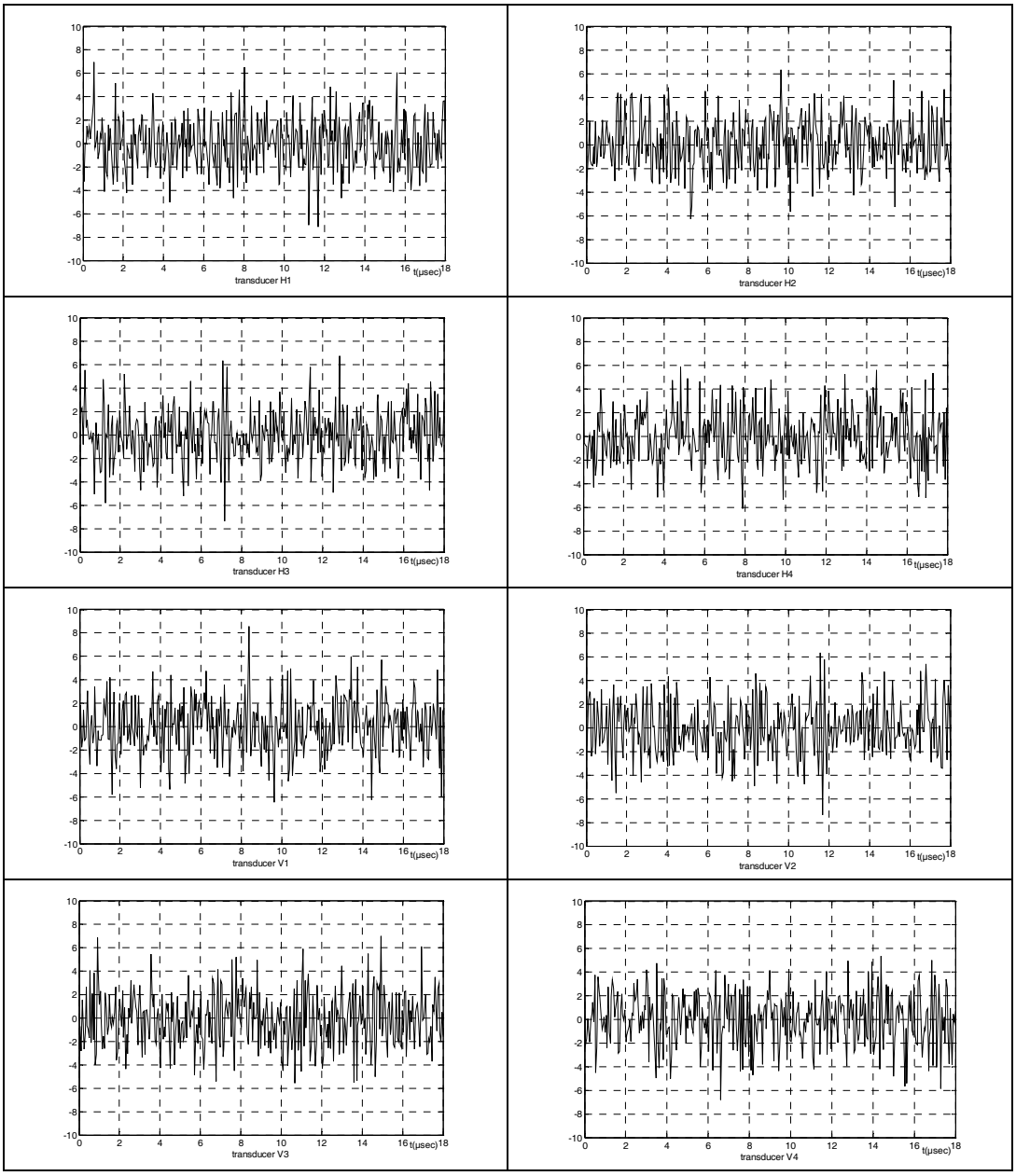

a)

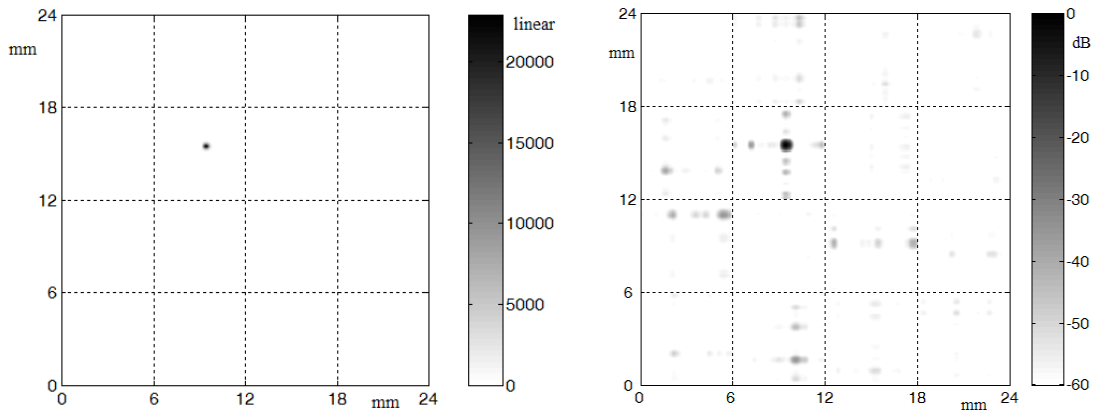

b) c)

Figure 5. The 2D location of a punctual flaw obtained using the wavelet fusing method. (a) Initial synthetic traces from 8 transducers with SNR_{ini} = 3 dB. (b) and (c) 2D flaw location displays for the overall test piece (16 cells, 24 x 24 mm), using linear and logarithmic scales, respectively.

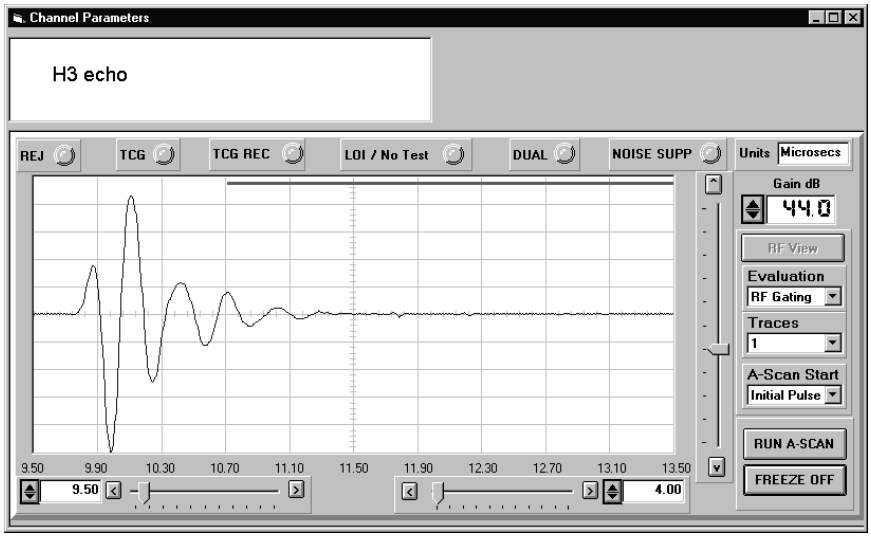

a)

b)

Figure 6. The A-scans from transducers H3 (a) and V2 (b) using the experimental setup shown in figures 2 and 3.

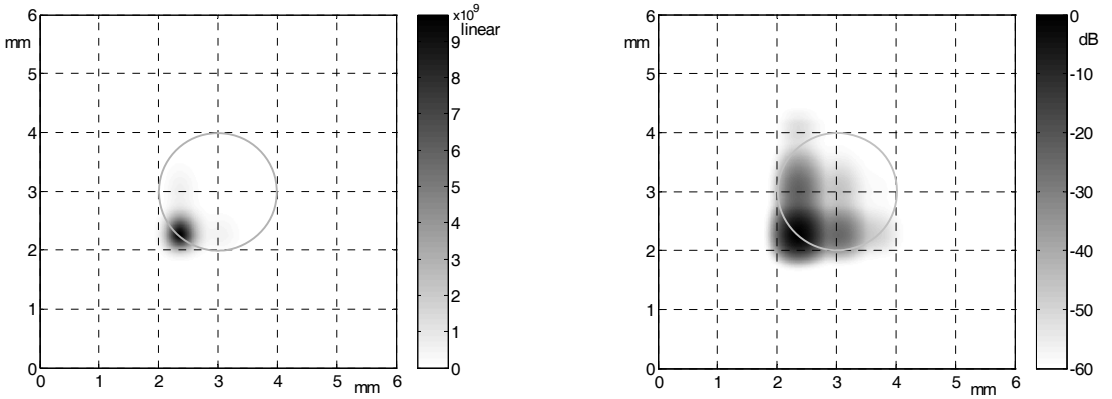

Figure 7. 2D displays of the inspection results from the H3-V2-intersection elemental cell (6x6 mm) of the methacrylate sample containing a 2mm circular hole, after processing the experimental traces using the UWPT fusing method. Zooms of the cell inspection using: (a) linear and (b) logarithmic scales.

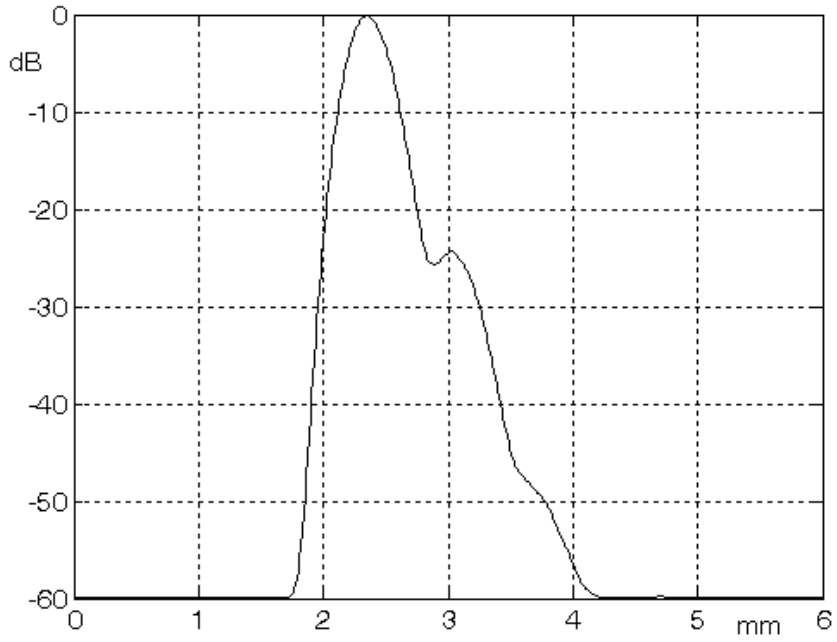

Figure 8. 1D profile of a horizontal cross-section in figure 7.b at a height of 2.3 mm (the maximum value line in 2D display). A small lateral "lobe" at a distance of 0.7 mm from the peak can be appreciated.

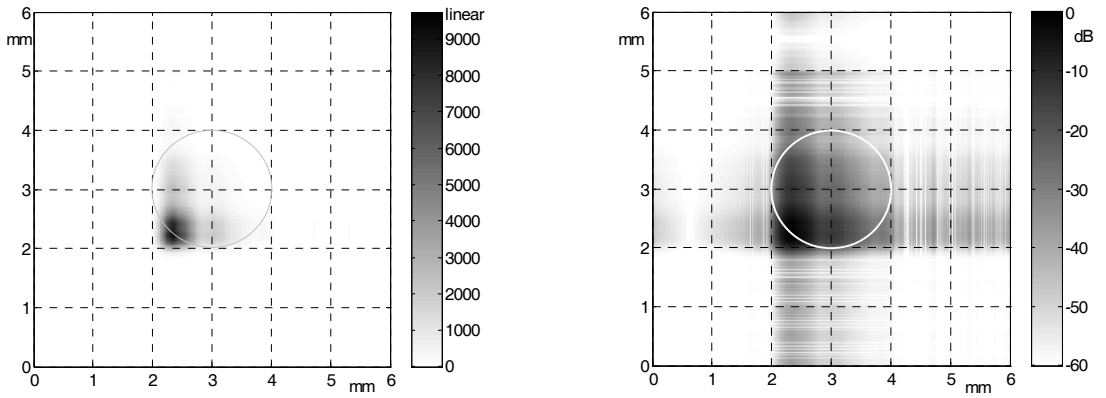

Figure 9. A zoom of the 2D representation of the H3-V2 elemental cell (6x6 mm) containing a 2 mm hole, using the direct time-domain combination method: with linear (a) and logarithmic (b) scales.

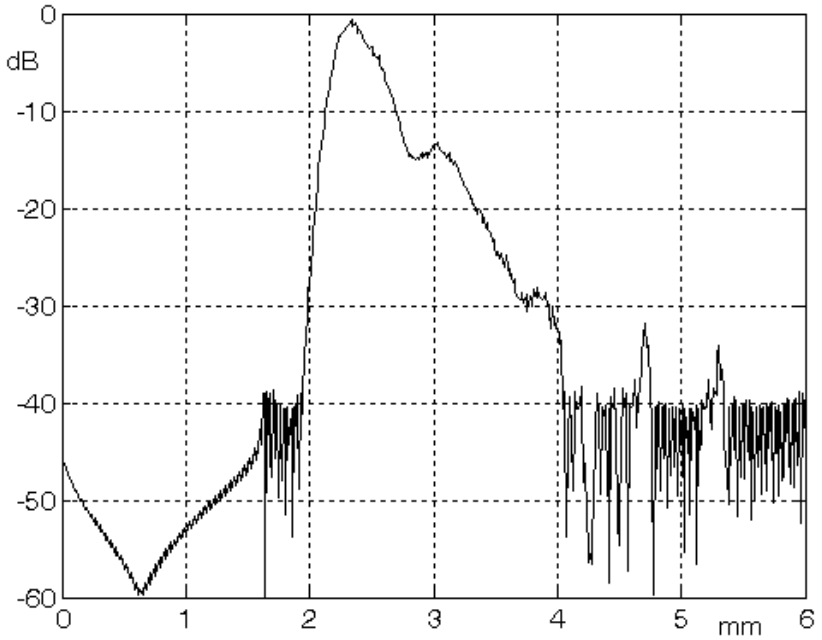

Figure 10. The 1D profile corresponding to the horizontal section taken from figure 9.b at a height of 2.3 mm (line of the maximum value in 2D display). A number of small lateral lobes (located between 3 and 6 mm) can be seen; the largest, at 3 mm, has a significant amplitude of -13dB.

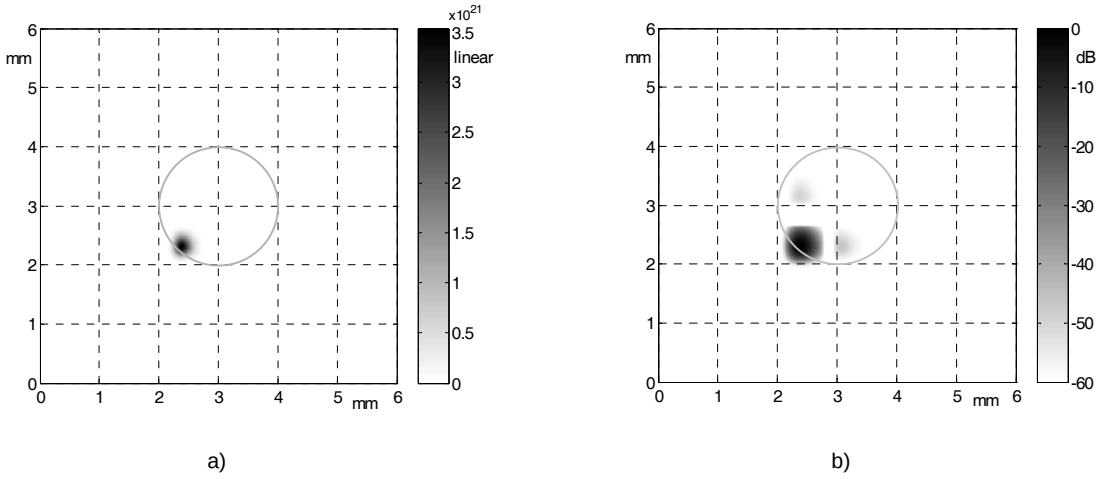

Figure 11. A zoom of the H3-V2 elemental cell (6x6 mm) with a 2mm hole: location results as in Figures 7 and 9, but using the Wigner-Ville combination method, with linear (a) and logarithmic (b) scales.

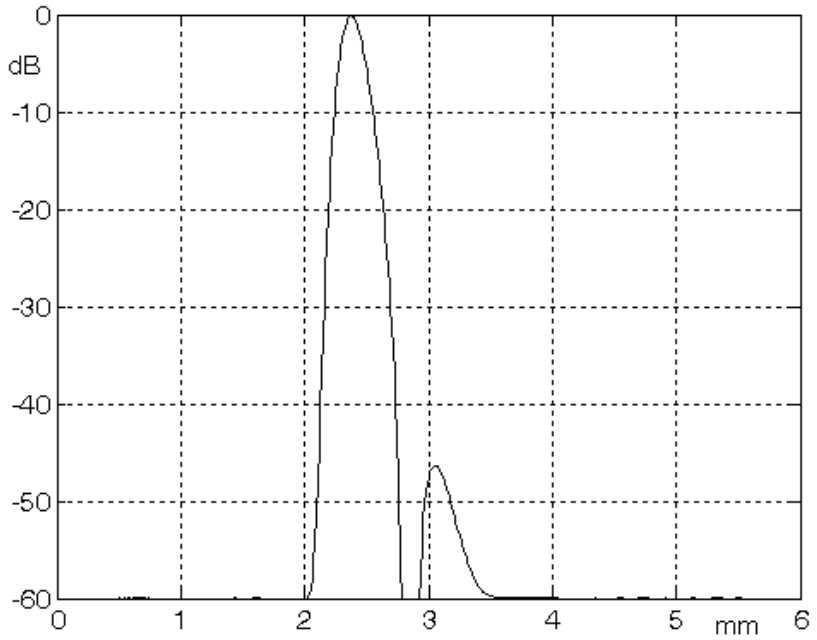

Figure 12. The 1D profile corresponding to a horizontal section of figure 11.b (with logarithmic scale), at a height of 2.3 mm (line of maximum value). A small lateral "lobe" separated from the main lobe is seen.